Bulgarian Academy of Sciences. Space Research and Technology Institute.
Aerospace Research in Bulgaria. 36, 2024, Sofia

DOI: https://doi.org/10.3897/arb.v36.e05

ON THE DELAY OF THE ADDITIONAL MORTALITY LINKED TO THE GEOMAGNETIC DISTURBANCES

Tsvetan Georgiev, Siyka Simeonova, Luba Dankova[1]

[1]Institute of Astronomy and National Astronomical Observatory – Bulgarian Academy of Sciences
e-mail: tsgeorg@astro.bas.bg

Keywords: *Geomagnetic disturbances, Sun- mortality relationship*

Abstract

Geomagnetic disturbances, mainly geomagnetic storms (GMSs) but also low-frequency resonances, touch some people susceptible to cerebrovascular diseases (CVDs). Sometimes, the geomagnetic effect is overestimated speculatively. Against this concept, we compare the changes of geomagnetic indexes (GMIs) with the changes of the additional mortality rate (AMR). We compared employing cross-correlation functions (CCFs) and use the Wolf number (WN) as a referent time scale. We suspect that strong GMSs, like these in 2003, increase the relative common MR 3–4 years later by up to 4×10^{-5}. Otherwise, the typical GMS-linked AMR seems less than 10^{-5}. Even if these values are overestimated, generally, they are small. Analyzing data about Bulgaria and five of its regions for the last Solar cycles, we confirm that the lag of the maxima of the GMS-linked ANR behind the WN maxima is ~5 years. We also confirm that the lag of the GMSs maxima behind the WN maximum is 1–2 years. We found that the lag of the maxima of the CVD-linked AMR behind the maxima of the GMSs is 3–4 years. So, we consider the 5-year lag of the AMR linked to the GMSs behind the WN maximum appears a sum of two delays mentioned above, 1–2 years and 3–4 years. In principle, the typical duration of CVDs may be derived if the beginnings are known. In medicine, they are usually unknown. However, suspecting the GMSs as triggers of a part of the CWD-linked AMR, we should suppose that these CWDs finish with lethal outcomes after 3–4 years.

Introduction

Usually, the moments of geomagnetic activity are referred to as the time scale of the Wolf number (WN). The WN W is defined as a relative number of sunspots. The number and the intensities of the high-energetic solar processes that affect the Earth correlate with the WN.

The changes of the speed and density of the solar wind (due to the flares and coronal mass ejections) cause geomagnetic disturbances (GMDs) for up to several hours. The GMDs, especially the geomagnetic storms (GMSs), affect many processes on Earth, including human health. The GMDs are characterized by geomagnetic indexes (GMIs, Section 2). The GMS maxima lags behind the WN

maxima by 1–2 years ([1], Figs. 17, 19; [2], Figs. 5, 6; [3], Fig. 1; [4], Fig. 3). In this work the lag of the GMS maxima behind the WN maxima is found to be also 1–2 years, see Figs. 4, right, and 6.

The proton concentration *Np* above the Earth's atmosphere is due mainly to the galactic cosmic rays varies. While the solar activity is high, the solar wind suppresses the galactic cosmic rays, and *Np* is low (effect of Forbush). When *Np* is high and variable, it creates low-frequency electromagnetic resonances (LFRs) in the chamber between the Earth's surface and the ionosphere (Schumann resonances). When the resonance frequency is very low, 1–2 Hz, it may be somewhat dangerous for the heart rhythm of some people [5, 6]. The LFR maxima lag behind the WN maxima, depending on the solar wind intensity, is 4–7 years. It takes place over and after the WN minima, see Figs. 2a and 6d.

The GMDs are linked to some health outcomes, connected mainly to the cerebrovascular diseases (CVDs) – coronary heart diseases, myocardial infarction (MI), brain stroke (BS), etc. GMDs are also linked to neurological system diseases, behavioral diseases, etc. In principle, CVDs cause half of the common mortality rate (MR) worldwide. However, in this paper, we concentrate on the additional MR (AMR) caused suggestively by the GMDs.

Usually, the studies concentrate on the correlation between solar activity and MIs and/or BSs. Many pieces of evidence exist about the negative influence of GMDs and LFRs on physiological and psychological human health [7–10]. For example, during days with GMS, the additional BSs and MIs suffer in Moscow, grow by 7.5% and 13%, respectively. (See the references of the Russian studies in [11]). It is also established that the GMDs caused by solar magnetic clouds are related to the increase in MI. The last-mentioned connection is higher than the GMDs caused by high-speed solar wind streams and on days with quiet geomagnetic activity [12].

Ionosphere and geomagnetic changes influence mortality from circulatory diseases. The CVDs' response to the changes in solar activity and abnormal solar events indirectly influence the concentration of electrical charges in the Earth's environment [13]. The different patterns in daily numbers of deaths during the quiet periods of solar activity are examined later. It is shown that there is a connection between the daily number of deaths and all indices of solar and geomagnetic activity in periods of low solar activity, in contrast to periods of strong solar storms [14].

The relationships between GMDs and the time course and lags of autonomic nervous system responses have been examined in [14]. It is confirmed that the daily nervous system activity responds to GMDs. The response is initiated at different times after the changes in the various environmental factors and persists over varying time periods. An increase in the solar wind, cosmic rays, solar radio flux, and Schumann resonance power was associated with increased heart rate and parasympathetic activity, interpreted as a biological stress response. The people are

affected in different ways depending on their sensitivity, health status, and capacity for self-regulation. The impact of short exposure to GMDs on total and cause-specific MR in 263 US cities has been investigated recently [3]. The GMDs and LFRs lead to an increase in city-specific and season-stratified common MR in all cities. The effects on total deaths were found in all seasons and on CVD and MI deaths – more in spring and autumn. These results may be explained through the direct impact of environmental electric and magnetic fields produced during GMDs and LFRs on the human autonomic nervous system.

In a review of the health effects of GMDs, Palmer et al. (2006) [16] reported five definite conclusions: (1) GMDs have a greater effect on humans at higher geomagnetic latitudes. (2) Unusually high geomagnetic activity seems to have a negative effect on human cardiovascular health. (3) Unusually low values of geomagnetic activity seem to have a negative effect on human health. (4) Only 10–15% of the people are negatively affected by GMDs, and (5) heart rhythm variations are negatively correlated with GMD. In this paper, we confirm that the lag of the AMR maxima behind the maxima of the WN is about five years, see Fig. 2. We propose an explanation of this "paradox". See our Summary.

Earlier, we found correlations of the cause-specific CVD AMR linked with GMSs for the Smolyan region of Bulgaria [11]. We found that concerning the years with low CMDs (1993, 1995, 1996, 1999), in the years with strong GMSs (2000, 2001, 2003–2005), the AMR is higher with 20–30% and the MR related to CVD is higher with 30–40% ([11], Figs.10–13). We also noted that the time delay of the maximum of the common and CVD AMRs in 2007–2008 takes place about 3–4 years behind the maximum of the strong storms in 2003–2005, see Fig. 1a. The increase in AMR and in common MR is about 50% and 5%, respectively. This result suggests that the influence of the GMSs on the AMR may manifest itself 3–4 years later. This is the motivation of the present work.

This paper reveals time delays of the AMR maxima by maxima positions of cross-correlation functions (CCFs). The CCF measures the similarity between the structures of two time series. It is a function of their relative lag time t_L, see Fig. 2 and 3. The large-scale trend in the series is an obstacle and must be removed preliminary. Fortunately, all time series used here pose linear large-scale trends. For example, in Fig. 2, we juxtapose the WN, W, and a few kinds of MR, M, after removing their linear fits. Thus, the CCF uses the deviations, for example, $\Delta W = W - W_F$ and $\Delta M = M - M_F$, where W_F and M_F are the relevant linear fits of the time series. The deviation ΔM is just the AMR.

So, in this work, the maxima positions of the CCFs are used to determine the time lags of the time series Θ, see Fig. 6 to 11. The CCF maximum is characterized by its value C and standard error σ_C. The CCF maxima in this paper are not high, often about 0.6, but their standard errors are relatively small. Then, the Student ratio $R=C/\sigma_C$ is usually high, giving evidence that the CCF maxima are significant, see Fig. 4 to 11.

Note that a graphical representation of the Student criterion for such cases as in [17], Fig. 4, shows how the threshold increases when the data number decreases. So, 20–10 data the 95% threshold is 0.6–1.1 and the 99% threshold is 0.9–1.6. Sometimes, our ratio *R* overcomes the threshold. Note also that the GMSs, LFRs, and CVDs have a highly complex origin and nature, which is out of the subject of this work. We are interested mainly in the cross-correlations between the deviations from the GMI fits (reasons) and the deviations from the MR fits (results), regarded as AMR.

Used abbreviations follow.

AMR – additional mortality rate;
BS – brain stroke;
CCF – cross-correlation function;
CVD – cerebrovascular disease;
GMD – geomagnetic disturbance;
GMI – geomagnetic index;
GM – geomagnetic storm;
LFR – low-frequency resonance;
MI – myocardial infarction;
MR – mortality rate;
NI – NASA (planetary) indexes (Section 2: *B, Kp, Ap, Np;* Fig. 5 and 6);
PI – Panagyurishte (local) indexes (Section 2: *Sa, Sb, Sc, Sn*; Fig. 4);
WN – Wolf number of the sunspots.

1. Data about the MR. Lags of the ANRs behind the WNs.

Figure 1 shows the behaviour of the habitant numbers *N* (circles) and MR*M* (dots) over the years. The numbers *N* are expressed in specific (implemented) units. The numbers *M* are always expressed per mile (in 10^{-3} *N*). Hereafter, the straight lines show the fits, while g and s are the gradient (slope coefficient) and standard deviation of the fit.

Figure la shows the initial data about the Smolyan region, Rodopi Mountain, between 1988 and 2008 [11] (Sun cycles 22+23). These data are valuable because they contain only the common MR M_1 and the medically confirmed CVD MR M_0. The data content follows:

N_1 – habitant number;
M_1 – common MR;
M_0 – MR linked medically with CVD;
M_D – residual MR, $M_D=M_1-M_0$.

The residual MR M_D corresponds to deaths caused by other reasons, including LFRs.

In the time episode of Fig.1a, N_1 decreases 1.3 fold, mainly due to young people's migration. Simultaneously, M_1 increases 1.5 fold, mostly because the

population gets older. The increases of M_0 and M_D are about 1.4 and 1.3 fold, respectively. In Fig.1a, two squares show an extraordinary maximum of the CVD MR M_0. Two large dots show respective deep minima in the residual mortality M_D. (The data marked by squares and dots do not participate in the relevant fits.)

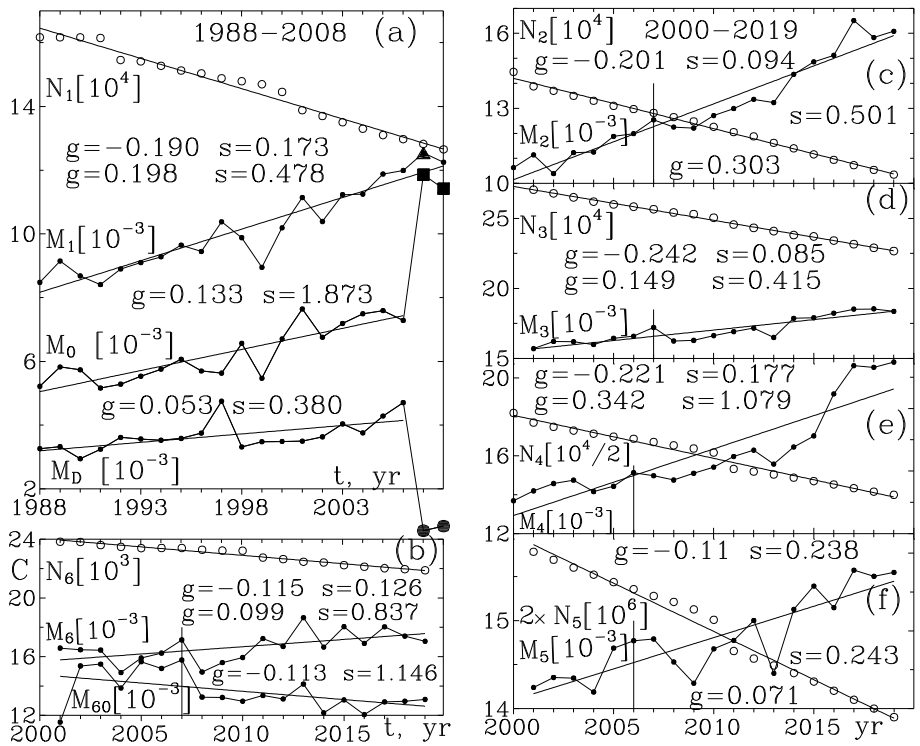

Fig. 1. Annual data about the habitants N and mortalities M for five Bulgarian regions plus Bulgaria as a whole. See the text at the beginning of Section 1.

Figures 1b–1f show five MR data systems for the time episode from 2000 to 2019 (Sun cycles are 23+24). The data source is the National Statistical Institute of Bulgaria [18]. The data content follows:

N_2, M_2 – again for Smolyan region, Fig. 1c;

N_3, M_3 – for Sofia suburb (without Sofia city), Fig. 1d;

N_4, M_4 – for the region of Dobrich plus Silistra together, Fig. 1e;

N_5, M_5 – for Bulgaria as a whole, Fig. 1f;

N_6, M_6, M_{60} -- for the eastern part of the Sofia suburb, Fig. 1b.

In the time episode of Figs. 1b–1f all habitant numbers N_2–N_6 decrease and all common MRs M_2–M_6 increase. The reason is the same as in Fig. 1a. The region in Fig. 1b (namely Elin Pelin) covers about 1/10 of the habitants of the Sofia

suburb, but it is also valuable here. It contains two kinds of common MR. M_{60} is recorded only inside the territory of this region, and it decreases. M_6 is the common MR, containing M_{60} plus the number of deaths of habitants of this region, but recorded in the nearby big hospital in Sofia. As expected, M_6 increases.

Let us return to Fig. 1. There, we may estimate the extreme and the ordinary AMR linked with the GMS. The extraordinary CVD MR M_0 in 2006–2007, after the strong GMSs in 2003, exceeded the local MR M_0 by ~50% (Fig. 1a). The relevant small peak in the common M_1 exceeds the local MR M_1 with ~4%. The vertical segments in Figs. 1b–1f mark the respective small local peaks of the common MR in 2006–2007 yr. The height of these peaks, including for Bulgaria as a whole, is up to ~4% above the local MR.

So, the strong GMSs (in this single case) seem to trigger an increase of the common MR up to ~ΔM =0.04×10^{-5} = 4×10^{-5}, with a time lag of 3–4 years. Otherwise, the typical CVD AMR, linked with GMSs, seems to be up to 1×10^{-5} per year. Because of unknown random AMR contributions, these AMRs seem to be overestimated, though. These AMR values seem to be negligible. For comparison, the number of deaths by car accidents for Bulgaria as a whole in 2017 is ~10×10^{-5}. Both values are overestimated and need justification.

The deviations of the MRs from the linear fits in Fig. 1a, ΔM_1, ΔM_0, or ΔM_D, are the AMR. After fit removal, these deviations participate in 3 important CCFs in Fig. 2a. They distinct the supposed contributions of CVD linked MR, common MR and common MR minus CVD linked NR LFR MR. The deviations of the MRs, ΔM_1– ΔM_5, clearly show the delay of the AMR linked with the GMDs with respect to the WN maxima.

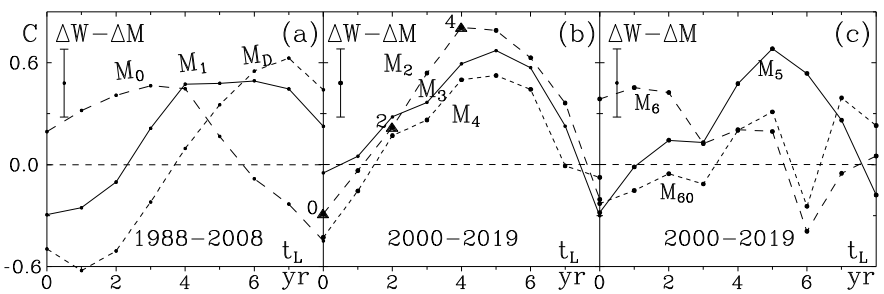

Fig. 2. CCFs between the changes of the WNs and fluctuations of the AMRs. The maxima position shows the delay of the AMR. See the text in Section 1.

Fig. 2 juxtaposes CCFs $C(t_L)$ between the WNs (shown in Fig. 5) and AMRs (shown in Fig. 1) over the time lag t_L. The CCF maxima mark the time lag of the AMR maxima behind the WN maxima. Note that linear fits of the compared time series are always removed. Vertical segments show the typical error bars of

the CCF values. Triangles in (b) mark the CCF values whose value deriving are illustrated in Fig. 3. Details about these graphs are shown in Figs. 7–11.

Fig. 2a shows the CCFs of WNs with the data M_1, M_0, and M_D from Fig. 1a. The CCFs have similar shapes. They show maxima lags behind the WNs of 3, 5, and 7 years, respectively. At about five years, the middle maximum corresponds to the common AMR. However, the maxima at 3 and 7 years may be linked to displays of CVD ANRs and LFR AMRs. In both cases, some additions of deaths for other reasons are present undoubtedly.

Fig. 2b shows the CCFs for the M_2, M_3, and M_4 data in Fig.1c–1e. The CCFs have similar shapes again. Their maxima show lags behind the WN for about five years. Hints of humps in the left parts of the CCFs, about a lag of two years, seem linked with CVD AMR. Triangles mark the CCF values derived as the coefficient of correlation, as illustrated in Fig. 3.

Fig. 2c shows by solid lines the CCF for the AMR of Bulgaria as a whole, M_5 from Fig. 1c. The shape is similar to the mentioned shapes of CCFs, with a peak lag of five years behind the WN. This CCF shows a local convexity at a lag of about two years, which ought to be linked with the contribution of CVD AMR. Figure 2c shows, by dashed broken lines, the CCFs for the common AMRs M_6 and the territory-bounded AMR M_{60}. These curves are very different. The left part of CCF for M_{60} is flat, as if CVD AMRs are missing. Obviously, a significant number of CVS AMP happen out of the territory, in the nearby big hospital. A remarkable hump is present in the left part of the CCF, only in the common AMR M_6. It seems CVD AMR dominates in this region.

In Fig. 2, the humps at lags of about five years behind the WRs contain contributions from the CVD, LFR, and other AMRs. It may be seen well in M_0, Fig. 2a, with a 2- to 4-year lag. In the other cases suspected, in M_2–M_5 with a lag of about two years and in M_6 with a 1- to 2-year lag.

So, if the strong GMDs are regarded as triggers of a part of the CVDs, with postponed lethal outcomes, then the lags of the GMD AMR behind the WNs, as well as the lags of AMRs behind the GMDs, may be revealed. In Section 2, we derived lags of GMIs behind the WNs. In Section 3, we showed details of deriving the CCFs, as shown in Fig. 2.

Fig. 3 shows the derivations of the CCF values at t_L-lags of 0, 2, and 4 years, marked in Fig. 2b by triangles. The top panels show the shifts of the shape of the WNs (thick broken lines) over the shape of AMR (thin broken lines). The linear fits of the compared series are removed. Here, n is the number of currently used points. Dashed broken lines show the useless edges of the time series after the shifts of WNs. The bottom panels show the respective correlation diagrams and CCF values C. Solid and dashed lines represent direct and reverse linear fits. Note that because of the large range of the WN, the compatibility of the graphs in the top panels is difficult. For this reason, the WN values $W'=W^{0.5}/20$ are used. This is

admissible because the values of the CCFs are dimensionless. Note that the values of *C* in the case (c_2), after a suitable mutual shift, become significant.

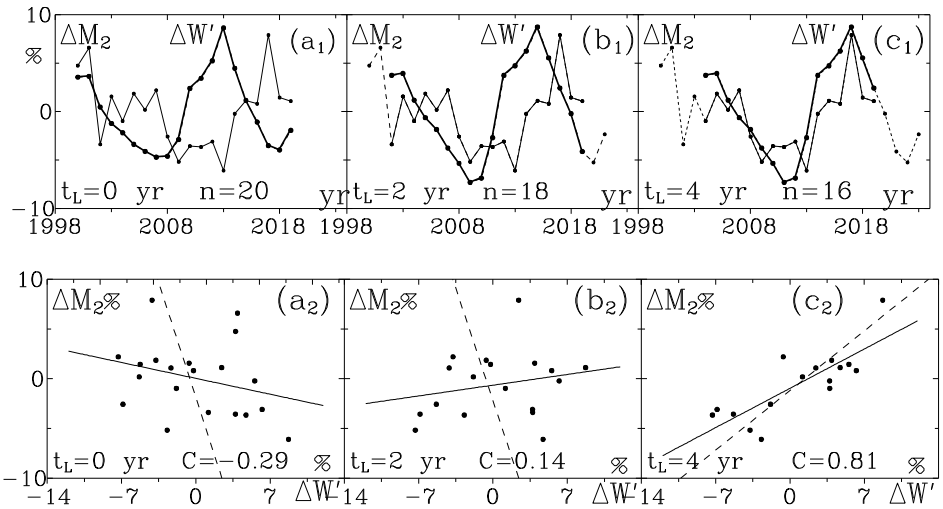

Fig. 3. illustrates the action of the CCF and the sources of the CCF values at points 0, 2, and 4 in Fig. 2b

2. Indexes about the GMDs. Lags of the GMDs behind the WNs

Initially, local GMIs in 1988-2008 were acquired from the Panagyurishte Geomagnetic Observatory of Bulgaria [11]. The Panagyurishte indexes (PIs) used here are derivatives of the measured vertical component *H* of the local geomagnetic field. The used annual PIs are:

Sa – average amplitude of all storms, in nT;

Sb – average amplitude of the moderate and strong storms, for *H*>120 nT;

Sc – average amplitude of *Sb*-type storms, but with sudden onset, in nT;

Sn – number of all storms.

Fig. 4 shows the behaviour of the PIs and their CCF with WNs. Figure 4, left graphs, represents the behaviour of the PIs and their trends over the years. Hereafter, *g* and *s* are the fits' gradient and standard error. The graphs cover the Sun cycles 22+23. In this episode, the everyday solar activity decreases (see Fig. $4d_1$ and $5a_1$–$5e_1$), but the large-scale trends of *Sa* and *Sb* are slightly positive. The powerful GMSs in 2003–2005 caused high peaks in the graphs of *Sa*–*Sc*. Fig. 4, the right graphs, show the CCFs $C(t_L)$ of the PIs with the WNs over the time lag t_L. Hereafter, Θ and *C* are the delay and the value of the CCF maximum. $R = C/\sigma_C$ is the Student ratio. The CCF maxima are relatively low and blunt. The time lags Θ of the CCFs maxima behind the WN maximum are 2, 1, 2, and 0 years,

respectively. Note that the number of all GMSs *Sn* reflects the general decrease of the solar activity and obeys the behaviour of the WN trend (Fig. $4d_1$, $4d_2$). The PI *Sn* is useless in the study of AMR delays. Therefore, we may consider the lag of the GMSs behind the WN maxima to be roughly two years.

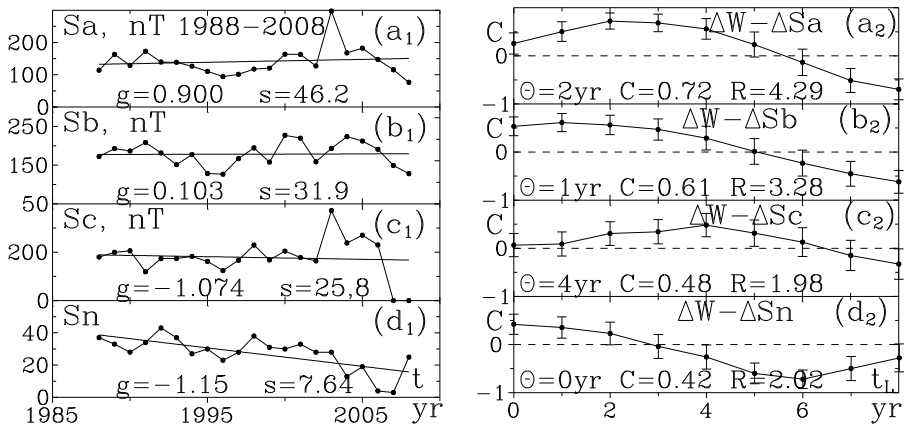

Fig. 4. PIs in Solar cycles 22+23 and their CCFs with the WNs. See the text.

We also used GMIs for 1988-2008 and 2000-2019 from the NASA website [19]. The NASA (planetary) annual indexes (NIs) used here are:

W – Wolf number of the sunspots;

Bm – the scalar value of the Earth's magnetic field, in nT;

Kp – GMI that characterizes the fluctuations of the electromagnetic field due to the GMSs;

Ap – GMI like *Kp* and approximately proportional to log *Kp*;

Np – proton concentration above the Earth's atmosphere, in cm^{-1}.

The NIs *Kp* and *Ap* indicate indirectly the powers of the GMSs. See [20].

Fig. 5 represents the behaviour of the NIs and their trends over 1988–2008 (cycles 22+23, left graphs) and 1998–2019 (cycles 23+24, right graphs). The right graphs show that the decrease of the common solar activity continues, but with decreasing Np in Fig. 5d2, it even increases weakly. The power storms in 2003 are observed as peaks in *Kp* and *Ap*.

Fig. 6 shows the CCFs of the Nis and the WNs. The CCFs pose again blunt maxima. The lags Θ of the NIs behind the WNs are 0, 0, 0, and 6 years in the left graphs and 1, 2, 2, and 4 years in the right graphs. The lags of the NIs *Bm*, *Kp*, and *Ap* behind the WNs in both cases may be considered to be between 0 and 1 year or 1 and 3 years. Further, the contributions of the AMRs, linked to different GMIs, will be regarded separately.

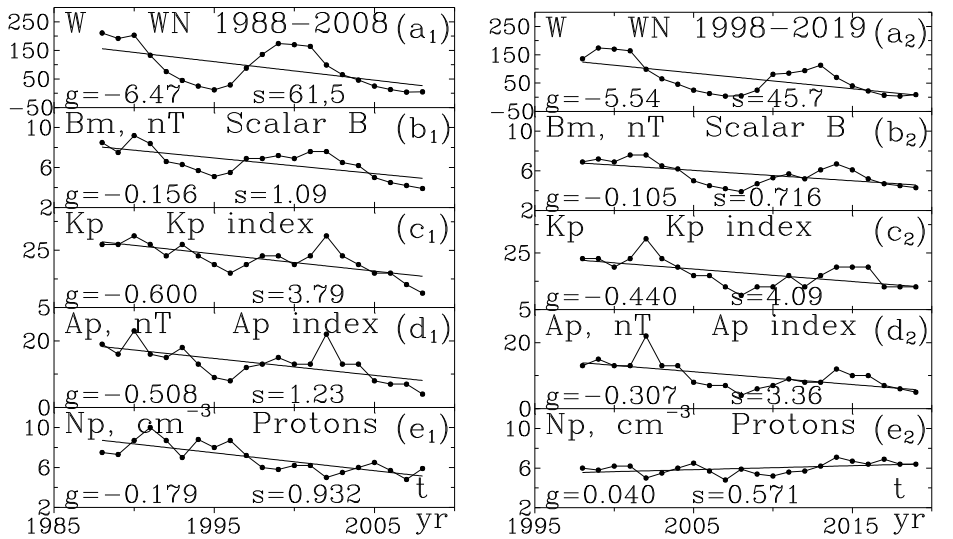

Fig. 5. NIs in Solar cycles 22+23 (left graphs) and 23+24 (right graphs). See Fig. 4, left graph, and the text.

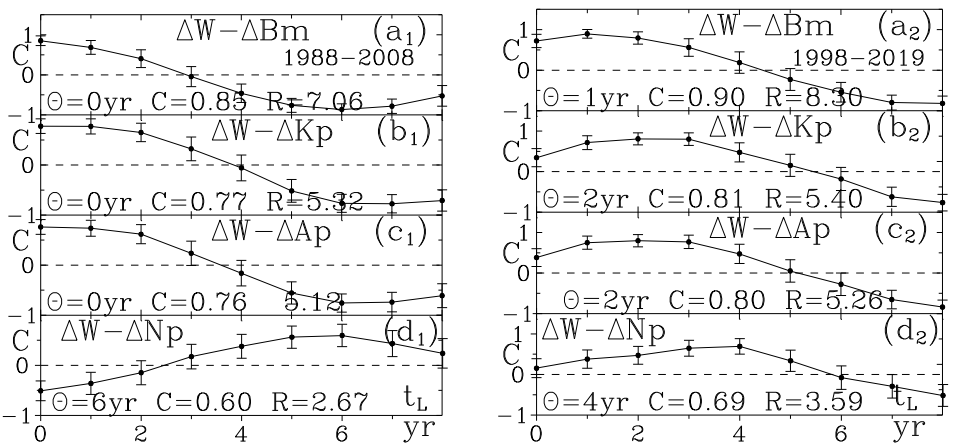

Fig. 6. CCFs between NIs and the WNs for 1988–2008 (left graphs) and for 1998–2019. See also Fig. 4, right graphs and the text.

The proton concentration *Np* is very interesting. Its maxima lags in Fig. 6d_1 or Fig .6d_2 behind the WN are from 5 to 7 years or 3 to 4 years, respectively. In Fig. 6d_1, this is the effect of higher solar activity (and higher Forbush effect). Then,

the LFR linked AMR contribution is distinct, as in Fig. 2a. In Fig. 6d$_2$, this is the effect of lower solar activity (and lower Forbush effect). Then, the LFR linked AMR contributes to the ordinary CCF maxima in Fig. 2a–2c, i.e., in the region of WN minima. For this reason, the maximum in M_2 in Fig. 2b is higher than the maximum in M_1 in Fig. 2a.

3. Lags of the AMRs behind the GMIs. Explanation of Fig. 2.

Fig. 7a to 7d show the CCFs between the common AMR M_1 and four GMIs for 1988–2006. The lags Θ of the AMR maxima are 4, 3, 0, and 5 years (left graphs with PIs) or 5, 5, 5, and 2 years (right graphs with NIs). Fig. 7e$_1$ and 7e$_2$ show the CCF between M_1 and WN (thick broken curve), as in Fig. 2a. Here, the beginning parts of the CCFs in (a)–(d) (thin dashed broken curves) are implemented. Note that the added curves are shifted to the right in accordance with their specific lags behind the GMI maxima in Figs.4b and 6a. So, the systems of added curves describe approximately the hump of the "main" CCFs (thick broken curves), better in 7e$_2$. The maximum of the common AMR is situated at ~5 yr behind the WNs maximum.

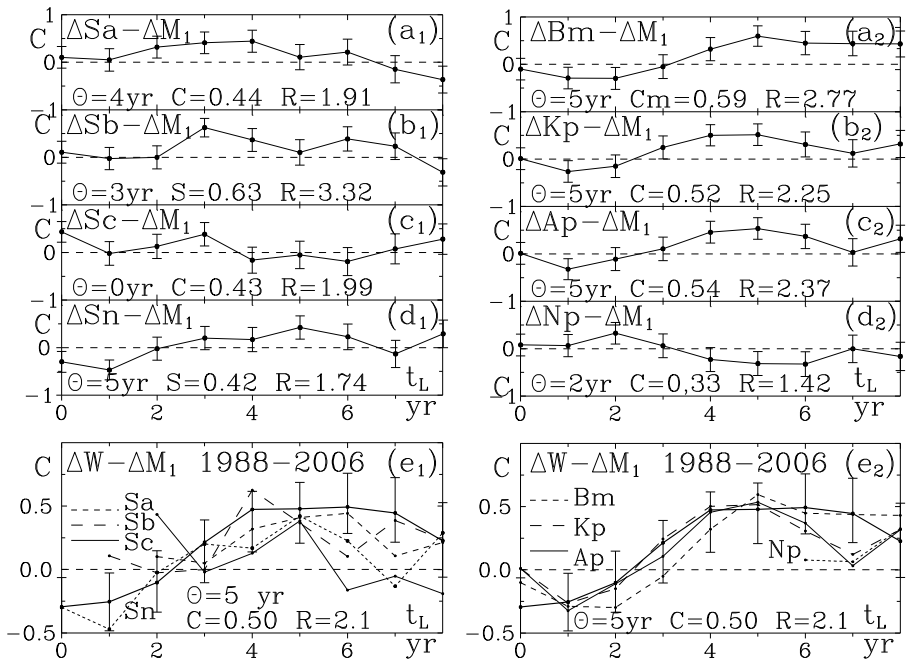

Fig. 7. CCFs for the common AMRs M_1 in Fig. 1a, with PIs (left graphs), NIs (right graphs) and WN (bottom graphs). See Fig. 4, right graphs and text.

Figures 8a–8d show the CCFs between the CVD linked AMR M_0 and 4 GMIs for 1988–2006. The lags Θ of the maxima are 0, 0, 0, and 3 years (left graphs, with PIs) or 3, 2, 2, and 7 years (right graphs with NIs). Fig. $8e_1$ and $8e_2$ show the CCFs between M_{10} and WN (thick broken curves), as in Fig. 2a. Similar to Figs. 7, the shifted beginning parts of the CCFs in (a)–(d) are implemented in (e) (thin and dashed broken curves). The systems of added curves again describe approximately the hump of the "main" CCFs (thick broken curves), better in $8e_2$. The maximum of the CVD linked AMR is situated at ~three years behind the WNs maximum. It seems that this hump contains a significant contribution from CVD linked AMRs.

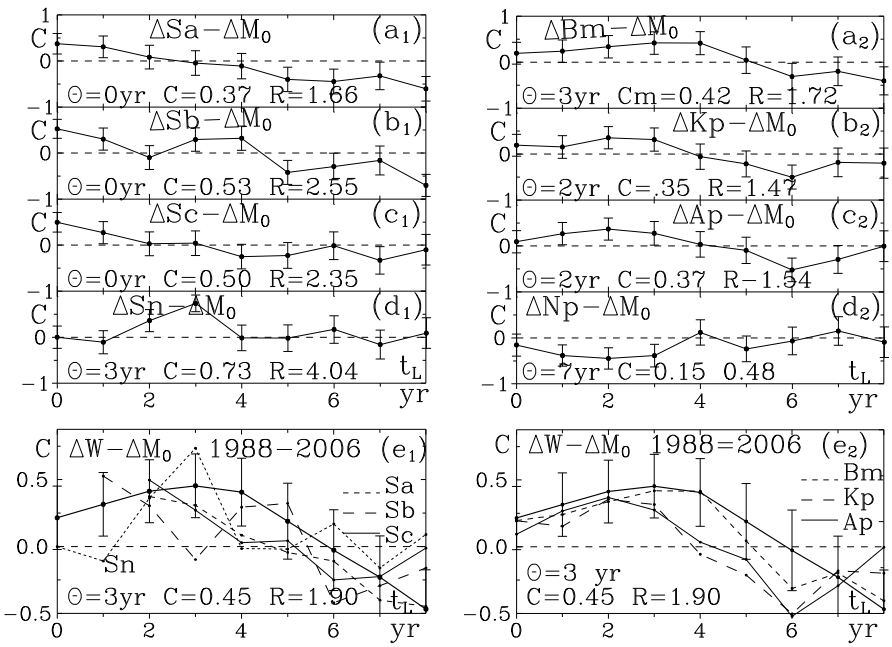

Fig. 8. CCFs for the CVD linked AMRs M_0 in Fig. 1a, with PIs (left graphs), NIs (right graphs) and WN (bottom graphs). See Fig. 4, right graphs and text.

Figures 9a–9d show the CCFs between the residual AMR M_D in Fig. 1a and four GMIs for 1988–2006. The lags Θ of the maxima are 3, 6, 3, 5 yr (left graphs) or 6, 4, 6, 7 (right graphs). Figures $9e_1$ and $9e_2$ show the CCFs between M_D and WN (thick broken curves), as in Fig. 2a. Similar to Figs. 7 and 8, the shifted beginning parts of the CCFs in (a)–(d) are implemented (thin and dashed broken curves). Again, the systems of shifted AMRs describe approximately the position of the hump in the "main" CCFs (thick broken curves), better in (e_2). The LFR

linked AMR's maximum is ~seven years behind the WNs maximum. It seems that this hump contains a significant contribution from LFR linked AMRs.

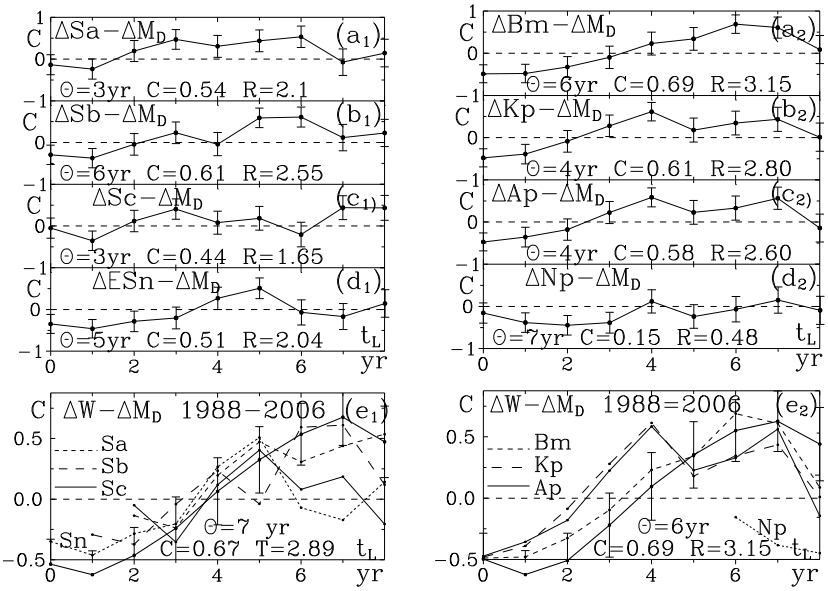

Fig. 9. CCFs for the LFR linked AMRs M_0 in Fig. 1a, with PIs (left graphs), NIs (right graphs) and WN (bottom graphs). See Fig. 4, right graphs and text.

Fig. 10 shows the CCFs between the common AMRs M_2 and M_3 with 4 NIs for 2000–2018. The lags Θ of the maxima behind the WN maxima are 3, 3, 3, and 2 (left graphs) and 3, 1, 3, and 2 (right graphs). The typical lag is ~three years. Again, the graphs in 10a–10d are implemented in 10e, shifted in respect to the lags behind their NIs in Fig. 6b. Obviously, the systems of added curves describe well the hump of the "main" CCFs (thick broken curves). The common AMRs' maxima in Figs.10e are 4 to 5 years behind the WN maximum.

Fig. 11 shows the CCFs between the common AMR M_4 and M_5 with four NIs for 2000–2018. The lags Θ of the maxima are 4, 3, 3, and 2 (left graphs) and 4, 4, 3, and 2 (right graphs). The typical lag is ~ three years. Again, the graphs in 11a–11d are implemented in 11e, shifted in respect to the lags behind their NIs in Fig. 6b. Obviously, the systems of added curves describe well the hump of the "main" CCFs (thick broken curves). The common AMRs' maximum is about five years behind the WN maximum.

The humps of the CCFs in Figs. 7e–11e1 which are explained here, are shown together in Fig. 2. These examples show that the lag of the AMR is about five years behind the maximum of the WN. Simultaneously, this lag may be regarded as a sum of two lags: a 1- to 2-year lag of PI or NI with respect to WN

plus a 3- to 4-year lag of the CVD linked AMR behind the CMIs. The hypothesis appears that the GMDs may be triggers of a part of the CVDs with a postponed lethal outcomes.

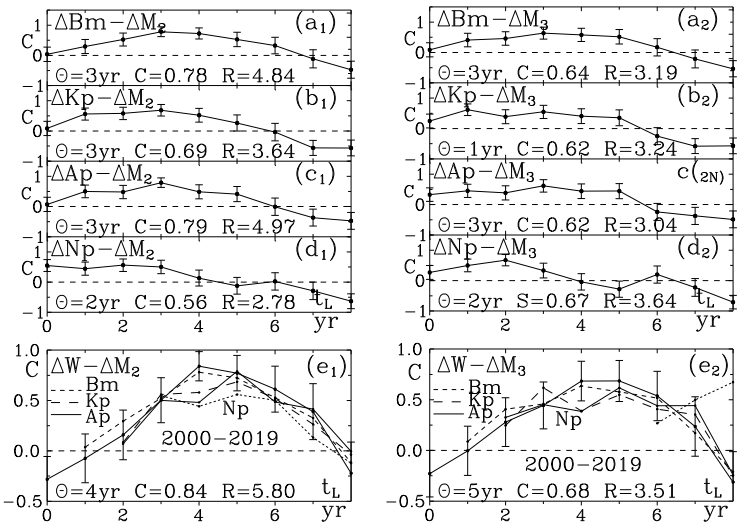

Fig. 10. CCFs for the common AMRs M_2 and M_3 in Fig. 1b, with NIs (left and right graphs), NI, and WN (bottom graphs). See Fig. 6, right graphs and text.

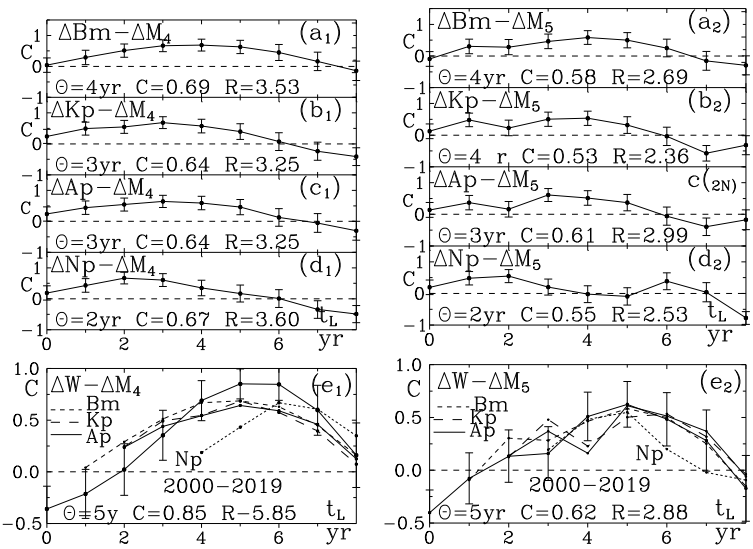

Fig. 11. CCFs for the common AMRs M_4 and M_5 in Fig. 1b and 1c, with NIs (left and right graphs) and WN (bottom graphs). See Fig. 6, right graphs and text.

4. Summary

The main results follow.

1. We confirm our suggestion in [11] that the strong GMSs in 2003 caused 3–4 years later, in 2006-2007, an annual increase of the CVD linked AMR with ~50% (Fig. 1a). The local increase in the common MRs is ~4% (Figs.1b–1f). Therefore, the strongest GMS may increase the common MR by about 4×10^{-5} with a lag of 3–4 years. Otherwise, the typical CVD linked AMR seems to be up to 10^{-5}.

2. Based on common AMR data M_1–M_5, for five regions, including Bulgaria as a whole, we showed that the shapes of the CCFs between WN and common AMR are very similar (Fig. 2). The lag of the maxima behind the WN maxima is about five years. So, the common AMR maxima fall on the WN minima, confirming consideration No.3 in [16] (see introduction).

3. We confirm that the lag of the GMSs maxima behind the WN maxima is 1–2 yr (Figs. 4b, 6). We find also that the lag of the CVD ANR maxima or LFR AMR maxima behind the WN maxima is 3–4 years or 4–7 years, respectively (Fig. 2 and 7–9). Therefore, consider the lag of the maxima of the common ANR behind the WN maxima, typically five years, which may be explained as a sum of the above-mentioned lags of 1–2 and 3–4 years.

4. Considering GMSs as triggers for CVDs, we estimated that the duration of the CVDs before the lethal outcome is typically 3–4 years. In medicine, the causes of CVDs are not known, and such direct estimation is impossible.

Acknowledgments

The authors thank Dr. B. Komitov for his attention and recommendations for this work.

References

1. Hathaway, D. H., (2010), Reviews in Solar Physics, Volume 7, The Solar Cycle (Springer).
2. Zerbo, J.-L., C. Amory-mazaudier, F. Ouattara, (2013), Adv. Res. 4/3, 265–274.
3. Zili Vieira, C. L., D. Alvares, A. Blomberg, et al., (2019), Environmental Health 18, No. 8 3.
4. Abe, O. E., M. O. Fakomiti,, W. N. Igboama, et al., (2023), Adv. Sp. Res. 71, 2240–2251.
5. Southwood, D., (1974), Planet. Sp. Sci. 22, 483–491.
6. Thayer, J. F., A. L. Hansen, E. Saus-Rose, et al., (2009) Ann. Behav. Med. 37, 141–153.
7. Friedman, H., R. O. Becker, C. H. Bachman, (1967), Nature 213, 949.
8. Gnevyshev, M. N., K. F. Novikova, (1972), J. Interdiscipl. Cycle Res. 3, 99.
9. Lipa, B. J, P. A. Sturrock, E. Rogot, (1976), Nature 259, 302.

10. Malin, S.R., C. Malin,, B. J. Srivastava, (1979), Nature, 277, 646
11. Simeonova, S. G., R. C. Georgieva,., B. H. Dimitrova, et al., (2010), Bulg. Astron. J. 14, 144–161
12. Dimitrova, S., I. Stoilova, K. Georgieva., et al., (2009), Fund. Sp. Res., HELIOBIOLOGY 161–165
13. Podolská, K., (2018), Journal of Stroke and Cerebrovascular Diseases} 27/2, 404–427.
14. Podolská, K., (2022), Atmosphere 13(1), 13.
15. Alabdulgader, A., R. McCraty, M. Atkinson, et al., (2018), Scientific Reports} 8, 1–14
16. Palmer, S. J., M. J. Rycroft, M. Cermack, (2006), Surv. Geophys. 27, 557–593.
17. Georgiev, Ts. B., (2014), Bulg. Astron. J., 20, 14–25.
18. https://www.nsi.bg/bg/content/2920/
19. https://omniweb.gsfc.nasa.gov/form/dx1.html.
20. https://www.ngdc.noaa.gov>stp>geomag>kp_ap

ВЪРХУ ЗАКЪСНЕНИЕТО НА ДОПЪЛНИТЕЛНАТА СМЪРТНОСТ, СВЪРЗВАНА С ГЕОМАГНИТНИТЕ СМУЩЕНИЯ

Ц. Георгиев, С. Симеонова, Л. Данкова

Резюме

Геомагнитните смущения, главно геомагнитни бури (ГМБи), но и нискочестотни резонанси, засягат част от хората, предразположени към мозъчни и съдови болести (МСБи). Понякога геомагнитният ефект се надценява спекулативно. Срещу това ние сравняваме изменения на геомагнитни индекси (ГМИи) и изменения на добавъчна смъртност (ДС). Ние правим това чрез кроскорелационни функции (ККФи), използвайки числото на Волф (ЧВ) за референтна времева скала. Ние подозираме, че силни ГМБи, като тези през 2003 г., увеличават 3–4 г. по-късно относителната обща смъртност с до 4×10^{-5}. Иначе, типичната ДС, свързвана с ГМБи, е под ~10^{-5} годишно. Даже ако тези наши величини са преувеличени, общо взето те са малки. Анализирайки данни за България и 5 нейни региони за последните 3 слънчеви цикли, ние потвърждаваме, че максимумът на ДС, свързвана с ГМБ, закъснява след максимума на ЧВ с ~5 г. Ние потвърждаваме и че максимумът на ГМБ закъснява след максимума на ЧВ с 1–2 г. Ние намираме специално, че максимумът на ДС, свързвана с ГМБи, закъснява след максимума на ГМИи с 3–4 г. По принцип, типичните продължителности на МСБи могат да бъдат определени, ако началата им са известни. В медицината началата са обикновено неизвестни. Обаче, подозирайки, че ГМБ са тригери на част от МСБи, ние следва да предположим, че тези МСБи завършват с летален изход след 3–4 г.